Journal of Traffic and Transportation Engineering(English Edition)
2014,1(5) : 362-370

Water flow simulation and analysis in HMA microstructure

Can Chen[1], R. Christopher Williams[2,*]

[1] *Graniterock Construction Company, Aromas, California, USA*

[2] *Department of Civil, Construction, and Environmental Engineering, Iowa State University, Ames, Iowa, USA*

Abstract: This paper introduces a new method for reconstructing virtual two-dimensional (2-D) microstructure of hot mix asphalt (HMA) . Based on the method, the gradation of coarse aggregates and the film thickness of the asphalt binder can be defined by the user. The HMA microstructure then serves as the input to the computational fluid dynamic (CFD) software (ANSYS-FLUENT) to investigate the water flow pattern through it. It is found that the realistic flow fields can be simulated in the 2-D microstructure and the flow patterns in some typical air void structures can be identified. These flow patterns can be used to explain the mechanism that could result in moisture damage in HMA pavement. The one-dimensional numerical permeability values are also derived from the flow fields of the 2-D HMA microstructure and compared with the measured values obtained by the Karol-Warner permeameter. Because the interconnected air voids channels in actual HMA samples cannot be fully represented in a 2-D model, some poor agreements need to be improved.

Key words: hot mix asphalt; microstructure; simulation; water flow

1 Introduction

HMA is a porous medium consisting of graded coarse and fine aggregates bound with asphalt binder plus a certain amount of air voids. In HMA pavement construction, it is important that the mix be adequately compacted in-place. If the air void content exceeds about 8 percent by volume, there may be interconnected channels which allow water to easily penetrate into the HMA pavement(Cooley et al. 2000; Brown et al. 2004) . High permeability could result in an increased potential for moisture damage in the pavement, such as raveling and stripping. However, such a phenomenon of moisture damage and water flow pattern in HMA pavement cannot be observed on a scale visible to the human eye. Computer simulation offers attractive opportunities for depicting the simulated internal HMA structure and studying the relationship between the pore mechanism and water flow characteristics in HMA.

There are a number of attempts in the literature dealing with the water flow simulation through HMA

* **Corresponding author:** R. Christopher Williams, PhD, Professor.
E-mail: rwilliam@ iastate. edu.

pavement structure and subgrade soil. Water flow and solid mechanical simulation in an actual HMA structure captured by 2-D and 3-D X-ray computer tomography images were successfully simulated by Al-Omari and Masad (2004), Dai (2011) and You et al. (2012). Wang et al. (2003) simulated the 2-D water flow in a dual-layer soil microstructure. However the parallel flow channel between clay particles used in their model is impossible to apply here for the HMA microstructure model because of the irregularity characteristics of the HMA internal structure. The effects of permeability and tortuosity of flow through sandy soil by the Lattice Boltzmann method were analyzed by Kutay et al. (2007) and Ghassemi and Pak (2011).

In this study, we first present a new method for reconstructing a virtual 2-D microstructure of HMA. Next, we model pressure driven flow through the HMA microstructure by ANSYS-FLUENT. Finally, the simulated flow field pattern is used to explain the moisture damage mechanism. The numerical permeability values are also calculated and compared with in-lab measured values at similar air void contents.

2 HMA microstructure reconstruction

There are basically two ways of numerically reconstructing porous structures: statistics driven reconstruction and process driven reconstruction (Ganapathysubramanian and Zabaras 2007). The process driven technique was selected in this study, since the statistics driven method needs an X-ray CT image database containing information such as the inter-air voids distance distributions and the number of air voids in a fixed area or volume, which are not available in the current phase of research. In recent decades, one of the process driven methods firstly developed by Wittmann et al. (1985) has been widely used for the visual simulation of concrete, HMA and other granular materials for its simplicity. More advanced models based on this method were studied in recent years (Schutter and Taerwe 1993; Gopalakrishnan et al. 2008; Zhang 2008). In their models, the coarse aggregates are assumed as either spherical or polygon shapes and then these aggregates are randomly packed in a fixed area or volume by Monte-Carlo method. However, the problems with this model are obvious. Firstly, the roles of fine aggregates and asphalt binder in HMA cannot be represented. Secondly, this model can only produce material structures with medium to high porosity, which is not very suitable for the simulation of HMA microstructure. To solve these problems, a new method for reconstructing 2-D HMA microstructure is proposed below.

Firstly, it is assumed that all coarse aggregates in the HMA have spherical geometries as the inner spheres shown in Fig. 1(a). The asphalt binder modeled by the outer circle is used to wrap the coarse aggregate particle/inner sphere and to glue with each other to form a larger and denser solid body. The thickness of the asphalt binder is assumed to be a function of the coarse aggregate dimension and is defined to be 15% diameter of the inner sphere. Further, if we consider the area wrapped by the asphalt binder as an inscribed sphere, then the convex polygon with a random-vertices number can be generated outside as shown in Fig. 1(b). The corner areas between the exterior polygon and interior sphere are relatively small and form different triangle-like shapes. Due to the irregular shape of the corner areas, they are considered as fine aggregates. The fine aggregate acting as a stone framework bonded outside the asphalt binder can closely reflect the HMA microstructure. Finally, the overlapped plot parts are merged together to create a whole patch as shown in Fig. 1(c) to form the simplest unit of a HMA microstructure. This reconstruction method combines the approaches proposed by Lu and Torquato (1992), Bagi (2005), and Li et al. (2009). Lu and Torquato (1992) treated all aggregate particles as spheres being dispersed in asphalt binder/liquid matrix and allowed them to achieve the desired positions according to equilibrium statistics. Li et al. (2009) took aggregate shape factors into consideration which can be used to establish a relationship between fine aggregates and asphalt film thickness here. The method proposed by Bagi (2005) created a higher density packing than most constructive methods existing in this literature. In order to simulate a HMA microstructure in a larger area, many units like the type shown in Fig. 1 should be compacted or packed together. The packing algorithm follows the rule that the asphalt binder-asphalt binder, as-

phalt binder-fine aggregate, coarse aggregate-fine aggregate, and fine aggregate-fine aggregate are all allowed to overlap with each other at their intersections but the coarse aggregate-coarse aggregate and asphalt binder-coarse aggregate are not allowed to do so (Fig. 1). Therefore, the inter-particle distances between the coarse aggregates can serve as the controlling parameter for particle positioning in the whole domain. The packing algorithm starts with placing numbers of largest coarse aggregates first at random positions and then smaller size coarse aggregates are added one by one in the empty space among the large aggregates. If the latter placed smaller coarse aggregate overlaps with a previous large one, then the smaller one would be rejected automatically, and another attempt would be made to place it. The HMA packing process is done when no more coarse aggregates can be placed into the domain.

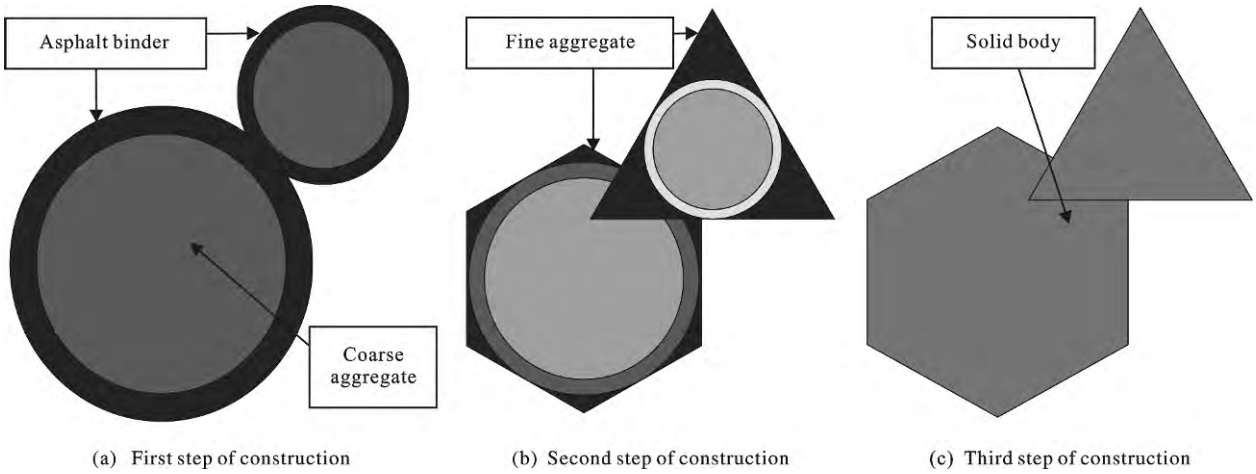

Fig. 1 Computer simulation of HMA solid body

The maximum aggregate size used for the simulation is 12.5 mm and aggregates larger than or equal to 4.75 mm (#4 sieves) are considered as the coarse aggregates. Therefore, there are three different sizes of coarse aggregates/inner spheres in this model: 12.5, 9.5, and 4.75 mm. The specific gravities for all aggregates are assumed to be the same in the simulation process. Then the gradation of the coarse aggregates can be controlled based upon their diameters rather than their retained weights on each sieve. Three different mixes are simulated based upon the gradation curve shown in Fig. 2. The targets are to generate the mixes with air void contents at around 8%, 12%, and 16%, respectively. Mix-2 with 9.5 mm nominal maximum size (NMAS) is first modeled and is served as a good base line mix for comparison with a total amount of 34 different sizes of coarse aggregates. Comparing with Mix-2, Mix-1 contains more 4.75 mm and less 12.5 mm particles, while Mix-3 with a 12.5 mm NMAS has more 12.5 mm and less 9.5 mm particles. However, the drawback of this HMA reconstruction model is that the gradations of fine aggregates are undeterminable since the fine aggregates are allowed to be merged within other parts. Therefore, their gradation curves are expressed by dot lines extending along the coarse aggregate gradation curves.

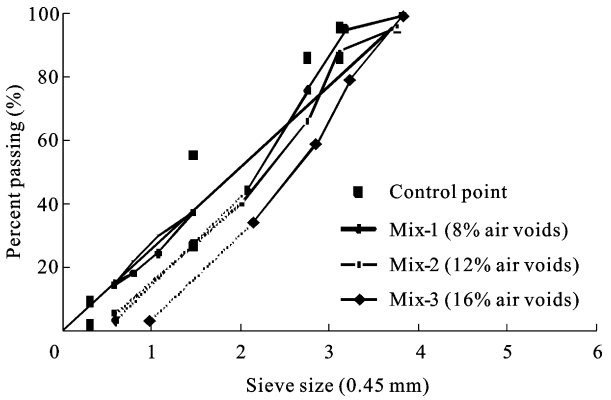

Fig. 2 Aggregate gradations for simulated HMA mixes

3 Water flow simulations and analysis

The visual HMA microstructures for Mix-1, Mix-2,

and Mix-3 are shown in Fig. 3. All three mixes are made in a 3.9 cm × 3.9 cm simulation domain. Simulated air void contents in the HMA microstructures are very close to the target air voids. Among the three mixes, the Mix-3 has the highest air void content and most complicated interconnected air voids channels, so it is chosen as a representative illustration of CFD simulation to understand the fluid flow characteristics in HMA. The simulated HMA air void contents can be calculated by Eq. (1)

$$\text{Air voids} = \frac{A_{\text{domain}} - A_{\text{soild}}}{A_{\text{domain}}} \times 100\% \qquad (1)$$

where A_{domain} is the simulation domain area; A_{soild} is the solid part area in the domain.

The HMA microstructure is meshed using triangular elements. Both global and local mesh controls in ANSYS are applied since the grid sizes need to be fine enough to resolve the flow field in narrow interconnected air void channels and at the same time coarse enough to cover the whole domain without requiring an infinite computational power. This finally results in 22800 total elements for the Mix-3 microstructure. The mesh is exported to the FLUENT solver through a journal file. A steady state laminar incompressible model is adopted for the flow regime inside our virtual simulation domain. The existence of flow motion in it depends on the hydraulic pressure gradient. Water is assumed to flow into the domain through a velocity-inlet (the top boundary) and leave it from the bottom and left boundaries. A symmetry boundary condition is used for the right side of the simulation box to double the domain area. Since permeability, as the intrinsic property of a porous material, is independent of water pressure gradient, arbitrary outlet pressure values are applied at the bottom and left boundaries. For the inlet condition, real mean inlet velocity values are used. They are obtained via the in-lab permeability test by the Karol-Warner permeameter on field HMA samples with the closest air void contents with the simulated ones. This ensuing section will further discuss how these field HMA samples are obtained. The Karol-Warner permeameter is chosen to measure the mean inlet flow velocity for its convenience to check how quick water can flow into the HMA by recording the drop of water level in a constant diameter stand pipe over a given time interval. The finite volume method implemented in FLUENT solver is exploited to solve the continuity and conservation of linear momentum for an incompressible continuum medium, such as water. For the simulation, FLUENT's "standard" scheme is used for the pressure interpolation and the "simple" scheme is used to represent the pressure-velocity coupling. To monitor the convergence of the simulation, the residuals are all down in the 1e-06 range in this study (ANSYS Inc. 2009).

Figure 3(c) shows the example of flow field in Mix-3 HMA microstructure. Magnitudes of flow velocity are illustrated in different colors. A brighter color shows a higher velocity. In this figure, the average breadth of the interconnected air void channel is about 1.25 mm with the narrowest path only 0.2 mm. Some more detailed flow patterns in the HMA microstructure are observed and discussed as follows:

a. The water flow velocity depends greatly on the size of air void channel, tortuosity and the channel orientation. For example, water has two paths (A and B) in Fig. 3(c). Higher velocity is observed along path B, which is broader and straighter. Obviously, a broader and straighter flow channel would result in higher permeability value in the local area from the view of micro-scale.

b. The existence of solid bodies reduces the area available for water flow. In order to preserve fluid continuity, water has to move through the micro-channels and hence increase the flow velocity in narrow necks.

c. Not all flow through porous media is laminar from the view of micro-scale. Many narrow and wide necks can be formed in the coarse air void channels. The top-left zoom-in view in Fig. 3(c) illustrates the interactive effect of the wide neck and narrow neck. Local boundary layer or even turbulent flow can be formed by the increased Reynolds number, since the narrow neck can lead to high speed flow in a porous medium and the wide neck can increase the hydraulic radius. This is one of the reasons for HMA moisture damage in pavement due to the non-uniform dynamic water pressure that will be further discussed.

d. The movement of flow in the HMA microstructure is not always downward but is a function of hydraulic pressure and channel orientation. Upflow is seen in the bottom-left zoom-in view of Fig. 3(c). Interconnected air void channels form a U-shape tube here. If the hydraulic pressure at the right side of the tube is larger than the left side, upflow can occur at the left side.

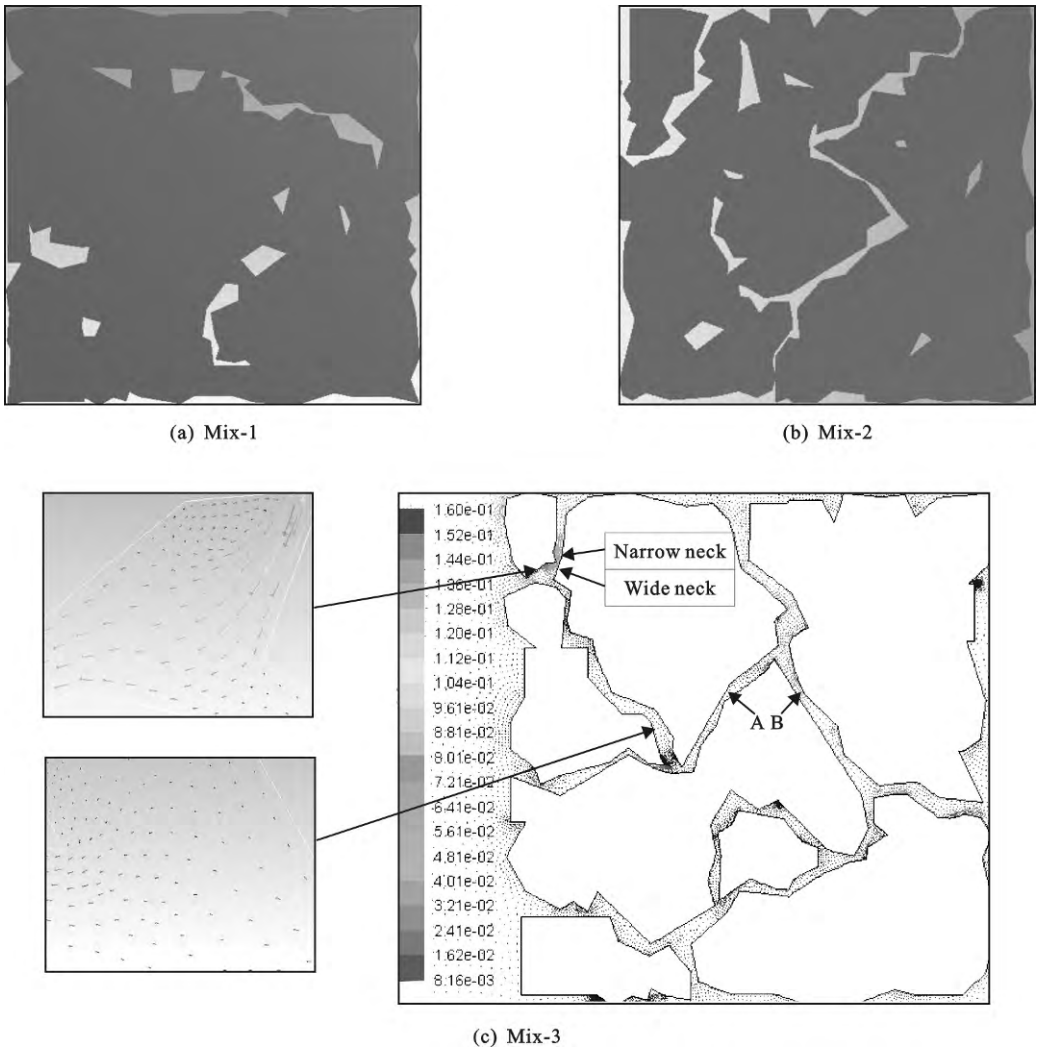

Fig. 3 Water flow simulation in a 3.9 cm × 3.9 cm HMA microstructure

As mentioned above, the flow velocity would increase through the narrow necks. This flow pattern is very important from an engineering point of view. Relatively high velocity (and momentum) would produce high dynamic pressure which represents the fluid flow kinetic energy. As the dynamic pressure increases the collision between water flow and solid bodies would be more forceful. In addition, in the non-slip condition higher laminar flow velocity would increase the wall shear stress because the velocity gradient near the wall/solid body would become greater. Wall shear stress is also obvious in turbulent flow. As the velocity of fluid further increases, fluid is sheared across the surface of the body, instabilities would develop and eventually the flow transitions into boundary layer or turbulent motion. Figs. 4 and 5 show the plots of dynamic pressure and wall shear stress distribution in three typical kinds of air void structures identified from the Mix-3 HMA microstructure. A brighter color shows a higher value. The same pressure difference is applied to form the flow fields in the three typical air void structures.

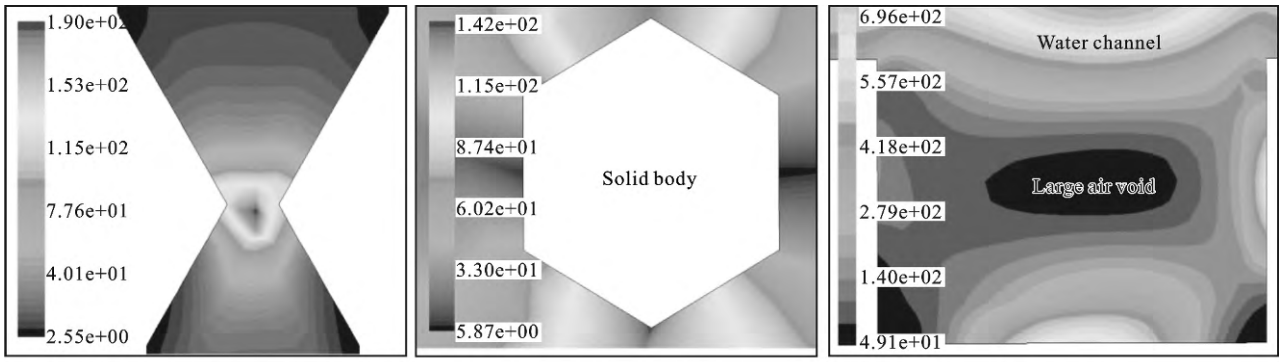

(a) Flow through narrow neck (b) Flow around solid body (c) Cavity flow

Fig. 4 Contours of dynamic pressure in different shapes of interconnected air voids

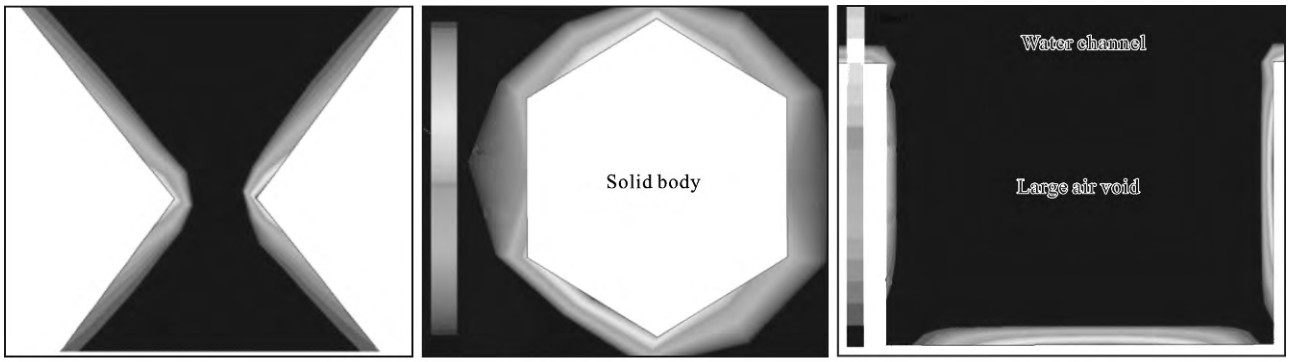

(a) Flow through narrow neck (b) Flow around solid body (c) Cavity flow

Fig. 5 Contours of wall shear stress in different shapes of interconnected air voids

Figures 4(a) and 5(a) show the dynamic pressure and wall shear stress distribution at a typical sharp-edged narrow neck. The greatest value of dynamic pressure is seen at the edge area. As mentioned above, our model idealizes the fine aggregates as 2-D triangular structures (the sharp edges) bonded with the asphalt binder. It is believed that flow-accelerated erosion would be the most evident in areas of high wall shear stress and dynamic pressure. This shape offers a numerical modeling framework that can be used to explain one of the leading phenomenons to moisture damage in HMA pavement. In a wet condition and under heavy traffic load cycles, water in air void channels of HMA structure would repetitively crash into the surface of fine aggregates and progressively weaken the adhesive bond between the asphalt binder and aggregates. Moisture damage caused by reduction in the cohesive bond between the asphalt binder and aggregates would be the last result. Further, another two kinds of air void structures that can be generated by our visual microstructure model are also used to investigate the potential for HMA moisture damage. One is water flow around a hexagonal solid body in the vicinity of two fixed plates; another one is the turbulent flow in a square cavity. Figs. 4(b) and 5(b) clearly show that along the direction of the fast moving fluid the greatest dynamic pressure and wall shear stresses occurring at the edge parts. The distributions of pressure and stress pattern are similar to that of the narrow-neck case in Figs. 4(a) and 5(a) . For the square cavity flow case, the pressure distribution would be somewhat different as shown in Figs. 4(c) and 5(c) . The square cavity can be considered as a large individual air void linked by other smaller interconnected voids. Flow in the interconnected air void channel would likely remain laminar, but local erosion due to turbulent flow can be formed in the cavity area. Turbulent flow can expand the space of the large individual air void by eroding the right side and bottom of the walls (Figs. 4(c) and 5(c)) . It is also noticed that the erosion part is the asphalt binder in our HMA model.

Finally, the calculation of the permeability value in the HMA microstructure is discussed here. In macro-scale, water flow in HMA sample follows the Darcy's law that the hydraulic pressure loss increases linearly with the velocity of water transmitted through HMA as long as the flow of water is laminar. Darcy's permeability tensor in the vertical direction through a porous medium can be determined by Eq. (2)

$$\frac{\partial P}{\partial y} = \frac{\gamma}{K_{yy}} U_y \tag{2}$$

where $\partial P/\partial y$ is the pressure gradient in the vertical direction; γ is the unit weight of the fluid; U_y is the average vertical flow velocity in the porous medium; K_{yy} is the Darcy's permeability tensor in vertical direction (cm/s).

However, from a micro-scale, the Darcy's law may not be used, since the water flow is highly irregular and not evenly distributed in torturous channels of a HMA microstructure. The permeability value obtained in Eq. (2) is the local permeability value and can only represent the viscous resistance effect on a very limited area within a porous medium. The values of local permeability obtained from micro-scale modeling need to be close to Darcy's permeability values from the macro-scale measurement in order to be used in practical applications. Obviously, the local permeability would be approaching Darcy's permeability if one could simulate out the entire structural size of the HMA in the micro-scale modeling and this is the reason why the 3.9 cm thick simulation domain is applied in our study. The HMA core samples taken from the field for the comparison of permeability values are all around 3.81 cm in thickness and 10 cm in diameter. Since the vertical boundary of the simulation domain is set to be the line of symmetry, the simulation box increases to 3.9 cm × 7.8 cm. As can be seen, the domain size is close to the real sample size and can reduce the difference between the simulated permeability value and real measured permeability value.

The simulated permeability values in the vertical direction are calculated by Eq. (2) with the measured top inlet flow velocity, arbitrary bottom pressure and simulated inlet pressure, bottom outlet velocity. The permeability values are shown in Fig. 6. It should be noted that the numerical permeability values in horizontal direction are unable to obtain since the Karol-Warner permeameter cannot be used to measure inlet flow velocity and permeability value horizontally. In order to compare the permeability values obtained in the simulated HMA microstructures with those in real HMA samples at similar air void content, roadway HMA core extractions were made at random locations along the longitudinal joint of Highway-6 in Iowa. It is generally believed that the longitudinal joint would be less dense than the rest of the lane away from the joint and has higher air void contents which would be closer to the level of air void contents in simulated HMA microstructures. Then the cores were transported to Iowa State University for subsequent air void and permeability tests by the Corelok® system and Karol-Warner permeameter, respectively. Finally, three field core samples with the air void contents closest to the simulated HMA microstructures were chosen for permeability comparison.

Figure 6 shows that as the air void increases, the relationship between the Karol-Warner permeability value and air void content would be no longer linear. A similar trend was observed by Harris (2007), Williams et al. (2010), and Chen et al. (2013). However, the simulated permeability values seem not follow the trend of the real permeability value and are much lower than the real ones. Reasons contributing to the result could be as follows. First, the permeability test depends on the interconnected nature of air voids in HMA rather than that simply on the total percent of air voids. At 7.8% air voids content (Fig. 3(a)), no inter-connected air voids can be formed in the HMA microstructure based upon our HMA reconstruction method and hence no permeability value can be obtained. Another reason could be related to the position of boundary conditions. Research in CFD area indicates that too close inlet and outlet boundaries would result in inaccurate pressure and velocity predictions. The inlet and outlet boundaries considered for the permeability simulations for fibrous materials should be placed at a distance 10 times larger than the diameter of the fiber away from the domain to obtain a relatively accurate result. However, how far away they should be placed for the simulation of granular materials is not investigated. Both the top and bottom boundaries are placed 10 cm away from the 3.9 cm ×

3.9 cm HMA simulation domain based upon the requirement for fibrous media. This may also give inaccurate simulated pressure values. Finally, consideration should be taken into the nature limitation of the 2-D HMA microstructure. It is generally believed that interconnected air void channels can only be fully represented in a three-dimensional (3-D) system. A 2-D section of a 3-D HMA microstructure would contain more isolated air voids and underestimate the permeability value.

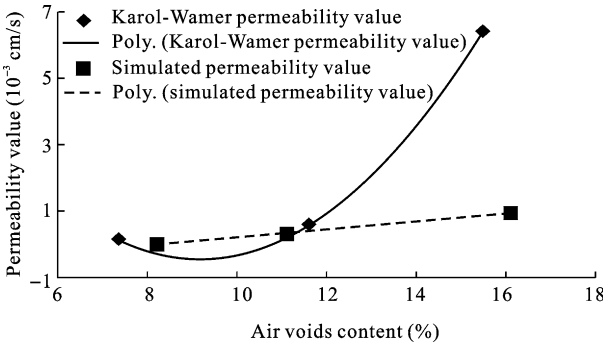

Fig. 6 Comparison of simulated and measured permeability values

4 Conclusions

In this paper, a new method for reconstructing virtual 2-D microstructure of HMA is presented. The computer simulation technique can randomly place the particles in double layer spheres and the spheres would be further expanded into polygon shapes in an area approximately equal to the sum of coarse aggregates, fine aggregates, and asphalt binder. Direct modeling of the water flow through the HMA microstructure is very complicated. This task was done in ANSYS-FLUENT commercial software which can accurately simulate the flow pattern in a given geometry. The flow pattern can be served to explain the mechanism of moisture damages in HMA pavement. The permeability values are also calculated out in post-processing work and are validated with laboratory measurements. It is found that our permeability calculation did not show a good agreement with the real laboratory results mainly due to the nature limitation of the 2-D HMA microstructure. This is because permeability is not just related to air voids. Tortuosity, shape of particles, void space are also significant factors. It is recognized that the results of this study as presented here are limited in terms of practical utility. The authors believe, however, that the application of particle packing simulation concepts to the study of aggregate structure in HMA in conjunction with the recent advances in X-ray tomography imaging techniques, 3-D simulation and discrete element modeling have tremendous potential to help us develop a deeper understanding of the HMA aggregate structure, develop and optimize the various parameters that describe the aggregate structure, and relate these parameters to the performance of pavements in a scientific way. This will provide the foundations to build more durable and long-lasting pavements.

References

Al-Omari, A., Masad, E., 2004. Three dimensional simulation of fluid flow in X-ray CT images of porous media. International Journal for Numerical and Analytical Methods in Geomechanics, 28(13): 1327-1360.

ANSYS Inc., 2009. ANSYS FLUENT 12.0 tutorial guide. ANSYS Inc., Canonsburg.

Bagi, K., 2005. An algorithm to generate random dense arrangements for discrete element simulations of granular assemblies. Granular Matters, 7(1): 31-43.

Brown, R. E., Hainin, R. M., Cooley, A., et al., 2004. Relationships of HMA in-place air voids, lift thickness, and permeability. NCHRP Web Document 68 (Project 9-27), Auburn University, Auburn.

Chen, C., Williams, R. C., Lee, H. D., et al., 2013. Quality control/quality assurance testing for longitudinal joint density and segregation of asphalt mixtures. Construction and Building Materials, 47(1): 80-85.

Cooley, L. A., Brown, E. R., Maghsoodloo, S., 2000. Developing critical field permeability and pavement density values for coarse-graded superpave pavements. Transportation Research Record, 1761: 41-49.

Dai, Q. L., 2011. Two and three dimensional micromechanical viscoelastic finite element modeling of stone-based materials with X-ray computed tomography images. Construction and Building Materials, 25(2): 1102-1114.

Ganapathysubramanian, B., Zabaras, N., 2007. Modeling diffusion in random heterogeneous media: data-driven models, stochastic collocation and the variational multi-scale method. Journal of Computational Physics, 226(1): 326-353.

Ghassemi, A., Pak, A., 2011. Pore scale of permeability and tortuosity for flow through particulate media using Lattice Boltzmann method. International Journal for Numerical and Analytical Methods in Geomechanics, 35(8): 886-901.

Gopalakrishnan, K., Shashidhar, N., Zhong, X. X., 2008. Study of compaction in hot-mix asphalt using computer simulations. World Academy of Science, Engineering and Technology,

2(3): 742-748.

Harris, C. H., 2007. Hot mix asphalt permeability: tester size effects and anisotropy. Master thesis, Virginia Polytechnic Institute and State University, Blacksburg.

Kutay, E. M., Aydilek, A. H., Masad, E., 2007. Estimating directional permeability of hot-mix asphalt by numerical simulation of microscale water flow. Transportation Research Record, 2001: 29-36.

Li, J. X., Williams, R. C., Marasteanu, M. O., et al., 2009. Investigation of in-place asphalt film thickness and performance of hot-mix asphalt mixture. Journal of Materials in Civil Engineering, 21(6): 262-270.

Lu, B., Torquato, S., 1992. Nearest-surface distribution functions for polydispersed particle system. Physical Review, 45(8): 5530-5544.

Schutter, G., Taerwe, L., 1993. Random particle model for concrete based on delaunay triangulation. Materials and Structures, 26(2): 67-73.

Wang, J. C., Leung, C. F., Chow, Y. K., 2003. Numerical solutions for flow in porous media. International Journal for Numerical and Analytical Methods in Geomechanics, 27(7): 565-583.

Williams, R. C., Raouf, M. A., Schroer, J., 2010. Alternative test methods for measuring permeability of asphalt mixes. The 89th Annual Meeting of Transportation Research Board, Washington DC.

Wittmann, F. H., Relfstra, P. E., Sadouki, H., 1985. Simulation and analysis of composite structures. Materials Science and Engineering, 68: 239-248.

You, T. S., Al-Rub, R. K., Darabi, M. K., et al., 2012. Three-dimesional microstructural modeling of asphalt concrete using a unified viscoelastic-viscoplatic-visodamage model. Construction and Building Materials, 28(1): 531-548.

Zhang, Y., 2008. Numerical simulation of dam concrete chemosmosis. http://www.paper.edu.cn/releasepaper/content/200811-769.